

Article

Response of Seismically Isolated Steel Frame Buildings with Sustainable Lead-Rubber Bearing (LRB) Isolator Devices Subjected to Near-Fault (NF) Ground Motions

Jong Wan Hu ^{1,2}

¹ Department of Civil and Environmental Engineering, Incheon National University, 12-1 Songdo-dong, Yeonsu-gu, Incheon 406-840, Korea; E-Mail: jongp24@incheon.ac.kr; Tel.: +82-32-835-8463

² Incheon Disaster Prevention Research Center, Incheon National University, 12-1 Songdo-dong, Yeonsu-gu, Incheon 406-840, Korea

Academic Editor: Derek Clements-Croome

Received: 4 September 2014 / Accepted: 17 December 2014 / Published: 24 December 2014

Abstract: Base isolation has been used as one of the most widely accepted seismic protection systems that should substantially dissociate a superstructure from its substructure resting on a shaking ground, thereby sustainably preserving entire structures against earthquake forces as well as inside non-structural integrities. Base isolation devices can operate very effectively against near-fault (NF) ground motions with large velocity pulses and permanent ground displacements. In this study, comparative advantages for using lead-rubber bearing (LRB) isolation systems are mainly investigated by performing nonlinear dynamic time-history analyses with NF ground motions. The seismic responses with respects to base shears and inter-story drifts are compared according to the installation of LRB isolation systems in the frame building. The main function of the base LRB isolator is to extend the period of structural vibration by increasing lateral flexibility in the frame structure, and thus ground accelerations transferred into the superstructure can dramatically decrease. Therefore, these base isolation systems are able to achieve notable mitigation in the base shear. In addition, they make a significant contribution to reducing inter-story drifts distributed over the upper floors. Finally, the fact that seismic performance can be improved by installing isolation devices in the frame structure is emphasized herein through the results of nonlinear dynamic analyses.

Keywords: lead-rubber bearing (LRB); base isolation system; frame building; inter-story drifts; base shear forces

1. Introduction

A number of catastrophic building failures due to severe and impulsive earthquakes have taken place worldwide since last few decades. In the aftermath of the 1994 Northridge and 1995 Kobe earthquakes, some scientists have raised special concerns as to ordinary buildings that are vulnerable to strong impulsive near-fault (NF) ground motions [1–3]. The NF ground motions recording from recent earthquakes are different from general ground motions in that they contain a strong-narrow band pulse of the spectral acceleration at short to intermediate periods [4–6]. Once ordinary frame buildings with relatively short vibration periods undergo these NF ground motions, inter-story drifts generated tend to be considerable due to strong ground acceleration pulses delivered into the column bases [7–10]. The implementation of seismic base isolation results in economical and practical solution that mitigates the magnitude of the seismic force by providing both lateral flexibility and energy dissipation through the insertion of the isolation device [11–15]. The base isolation systems conceptually pertaining to passive vibration control technologies contribute to shifting the fundamental (or natural) time period of the structure away from the high pulse of the spectral acceleration where the structures are mostly affected. Consequently, a basic scheme for adequately implementing the isolation system on the column base is to separate the main structure from the ground in an effort to avoid severe seismic damage.

The most common base isolation devices used over many years by engineers are lead-rubber bearing (LRB) isolators which combine isolation function and energy dissipation in a single compact unit [16,17]. Such LRB isolator devices provide vertical load support, horizontal flexibility, supplemental damping, and centering force to the structure from earthquake attack. In addition, they require minimal cost for installation and maintenance as compared to other passive vibration control devices [18,19]. The LRB isolator typically consists of laminated rubber layers with a lead core plug down its center as illustrated in Figure 1.

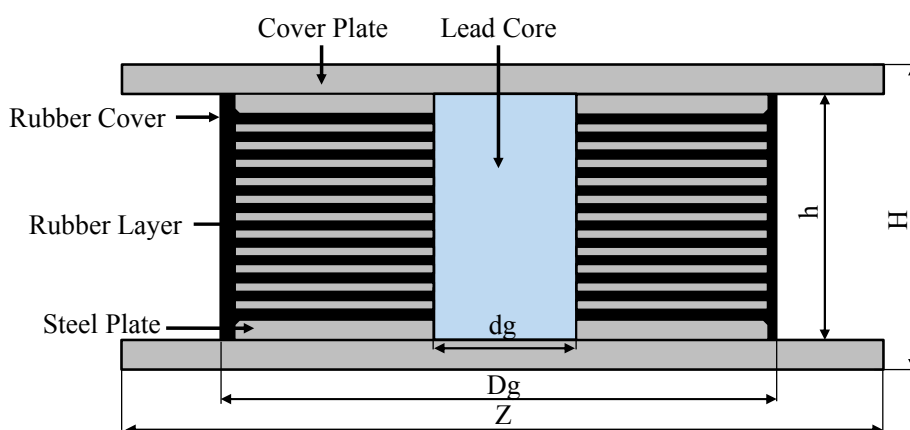


Figure 1. Typical lead-rubber bearing (LRB) isolator device.

The low damping elastomers constructed with elastomeric rubber bearings generally behave as an elastic manner toward external response. Thus, they can instantly supply isolation capacity, additional flexibility, and elastic recentering force to the LRB isolator device [20]. On the other hand, the lead core which yields at the relatively low shear stress responds with perfectly elasto-plastic loops, and hence offers not only sufficient energy dissipation but also supplemental damping component. The inner reinforcing steel plates stacked up constrain the laminated rubber layers from lateral expansion, and

provide high vertical stiffness resisting gravity loads. The typical LRB isolator has considerable maximum shear strains corresponding to between 125% and 200% because reinforcing steel plates have little effect on the shear stiffness. Therefore, the installation of the LRB isolator devices may be necessary for the frame buildings with an intention to mitigate structural damage.

A considerable amount of practical research associated with the use of this elastomeric LRB isolator has been conducted for several years. The early stage of research development has mainly focused on LRB responses estimated through experimental observations and numerical analyses, including LRB system design [21]. The stiffness models were developed to predict the force-displacement response of the LRB isolator device. On the other hand, recent researches have been trending toward the application of LRB isolation systems in the building structure [3,13–15]. The LRB isolators with hardening behavior were developed for low to mid-rise buildings located in the moderate seismicity area, and besides, the behavior of the base-isolated building was accurately predicted by nonlinear dynamic analyses performed with relatively long-period ground motions. Most recently, some researchers have been starting to evaluate seismic performance and capacity for the base-isolated multi-story building structure subjected to several NF ground motions [13–15]. Overall, NF ground motions produce strong acceleration pulses with undesirable effects on the response of the superstructures, thereby causing severe failure and instability in the superstructure. Accordingly, the LRB base isolators are required for building structures located on the NF sites in that they are very effective to reduce such ground accelerations transmitted into the superstructure. Notwithstanding that seismic performance for the base-isolated building under the NF ground motion leads many engineers and scientists to attract sufficient interest, there is a lack of proper research until now to implement the LRB isolator devices practically used in the actual frame building. Therefore, it is necessary to examine extensively the response of different LRB isolators with the combination of recentering and damping properties for the isolated steel frame building experiencing several NF ground motions.

This study is intended to mainly investigate seismic capacity and performance for LRB-isolated frame buildings located on the NF site area so as to address issues mentioned above. Two LRB isolator models used in the practical field are firstly selected for design and analyses. The mechanical properties of these isolator models, which are determined to comply with a recommendation specified in the common building design code [22–24], are introduced to reproduce their force-displacement responses. The LRB isolators presented herein are modeled as nonlinear component springs with the mechanical properties for the purpose of simulating isotropic hardening behavior during the analyses. The six story concentrically braced frame buildings with perimeter moment-resisting frames are designed in accordance with the current design guideline [22,24], and then modeled as two dimensional (2D) symmetric frame models. In this study, they can be classified as either LRB-isolated frame models or as-built frame models according to whether base isolation systems are installed or not. The individual frame models are evaluated with respect to seismic performance characterized by inter-story drifts and base shear forces after performing nonlinear dynamic time-history analyses with several NF ground motion records, and then compared to each other. Finally, statistical investigation based on analysis results should be conducted in order to fairly verify the effectiveness of the LRB base isolation system in the multi-story building structure.

2. LRB Isolator Devices

The LRB isolator is composed of an elastomeric bearing made by laminated rubber layers with steel shim plates, cover plates, and a lead core located on its center. The typical LRB isolator device is shown in Figure 1. This LRB isolator device can combine the function of isolation and recentering in a single unit (*i.e.*, elastomeric bearing), thereby giving structural support, horizontal flexibility, and recentering force to the isolation system [20,21]. Furthermore, it produces the required amount of supplemental damping and energy dissipation by adjusting the size of the lead core. The energy dissipation generated by the yielding of the lead core achieves an equivalent viscous damping coefficient up to approximately 30%, and effectively reduces the horizontal displacement. The LRB isolators are usually fabricated in circular sections, and sometimes produced with more than one lead core.

Two LRB models practically used in the construction field (*i.e.*, LRB1 and LRB2) are selected in this study. Including geometric details illustrated in Figure 1, mechanical properties needed to simulate their force-displacement responses are presented in Table 1. As shown in Figure 2, the force-displacement responses can be ideally modelled as bilinear hysteresis loops. The bilinear hysteresis loops considered herein are defined as four key parameters given in Table 1 per each LRB model, such that: yield displacement (Δ_1), yield force (F_1), specified design displacement (Δ_2), and its corresponding force (F_2). The elastic stiffness (K_e) and the post-yield stiffness (K_p) are also defined as the equations involved with these four parameters as follows:

Table 1. Properties of the LRB isolator models.

Model ID	Δ_{max} (mm)	F_v (kN)	F_1 (kN)	F_2 (kN)	Δ_1 (mm)	Δ_2 (mm)	Q (kN)	K_e (kN/mm)	K_p (kN/mm)	K_{eff} (kN/mm)	λ_{eff}	Z (mm)	D_g (mm)	d_g (mm)	H (mm)	h (mm)	t_e *
LRB1	400	3170	259	651	16	333	239	16.19	1.24	1.95	22.3%	800	750	170	397	337	203
LRB2	400	5780	308	823	16	333	282	19.25	1.62	2.47	20.8%	900	850	185	382	322	200

* Total thickness of the rubber.

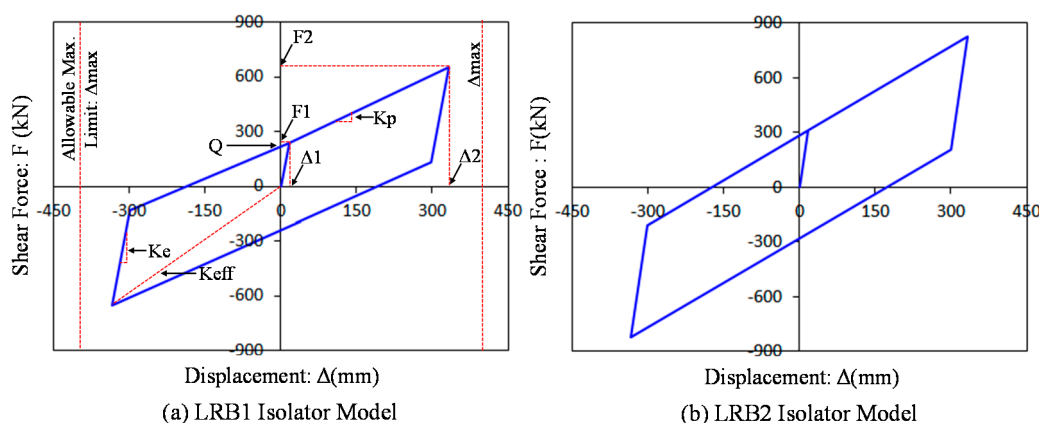


Figure 2. Hysteresis loops of the presented LRB isolator devices modeled as bilinear curves.

$$K_e = \frac{F_1}{\Delta_1} \tag{1}$$

$$K_p = \frac{F_2 - F_1}{\Delta_2 - \Delta_1} \tag{2}$$

The effective stiffness of the hysteretic behavior (K_{eff}) can be modelled the secant line by means of the ratio as in the following equation:

$$K_{\text{eff}} = \frac{F_2}{\Delta_2} \quad (3)$$

The characteristic strength indicating force-intercept at the zero displacement (Q) can be also expressed as the function of the post-yield stiffness as follows:

$$Q = F_1 - K_p \cdot \Delta_1 \quad (4)$$

The hysteretic loop area (E_{iso}) representing the amount of energy dissipation can be obtained from the equation as follows:

$$E_{\text{iso}} = 4Q \cdot (\Delta_2 - \Delta_1) \quad (5)$$

The effective viscous damping coefficient (λ_{eff}) is proportional to the amount of energy dissipation, but inversely related to both the effective stiffness and the square displacement. This damping coefficient also depends on four key parameters, which it refers:

$$\lambda_{\text{eff}} = \frac{E_{\text{iso}}}{2\pi \cdot K_{\text{eff}} \cdot (\Delta_2)^2} = \frac{2}{\pi} \left(\frac{F_1}{F_2} - \frac{\Delta_1}{\Delta_2} \right) \quad (6)$$

The mechanical properties obtained from calculations in the above equations are summarized in Table 1. The LRB2 model was designed with geometric parameters which are larger diameters and smaller heights, as compared to those of the LRB1 model. Owing to this parametric property, the slope of the LRB2 model which indicates the stiffness to resist horizontal displacement is overall stiffer than that of the LRB1 model. In addition to the stiffness, other properties such as force capacity, maximum allowable vertical load (F_v), and characteristic strength can be similarly affected by the size of the LRB model. In contrast, the LRB2 model exhibits slightly lower damping coefficient than the LRB1 model as expected in Equation (6). Both LRB models have the same maximum allowable horizontal displacement ($\Delta_{\text{max}} = 400 \text{ mm}$), representing 1.2 times the length of Δ_2 .

3. Frame Model and Design

All prototype buildings were designed in accordance with current design guidelines [22–24] so as to examine the effect of base isolation systems under earthquake events. They were assumed to be located on the stiff soil site (*i.e.*, site class D per ASCE 7-05 definition [24]) in the Los Angeles (LA) area, and be subjected to a 10% probability of exceedance in 50 year (10% in 50 years) seismic hazard corresponding to design-based earthquake (DBE). The seismic design category (SDC) class D is considered to be a high seismicity as stipulated in the ASCE 7-05 design code was applied for frame design. Including dead and live loads (DLs and LLs), basic design conditions are summarized in Table 2. The mapped spectral accelerations for 0.2- and 1-s periods were taken as 2.35 g and 1.41 g, respectively. The response modification factors were taken as the value of 6 consistent with concentrically brace frame (CBF) structures [22]. The sizes of structural members (*i.e.*, brace, beam, and column members) were designed in accordance with the AISC-LRFD manual [23]. A set of horizontal loads corresponding to the DBE force level should be generated on the basis of equivalent load transformation procedure in

order to perform initial frame design through 2D nonlinear pushover analyses. The inter-story drifts obtained from these analyses resulted in the significant design criteria. The member sizes for prototype frame buildings were revised until inter-story drift ratios could fulfill 2% allowable maximum limits [22,24]. Furthermore, P-delta amplification factors computed by using analysis results were examined whether stability limits could be satisfied or not.

Table 2. Basic conditions for frame design (DL: dead loads; LL: live loads).

Located Area	Loads (Other)	Loads (Roof)	SDC	Site Condition	Occupancy Category
LA Area	DL: 4.12kPa, LL: 2.39kPa	DL: 4.50kPa, LL: 0.96kPa	D Class	Stiff Soil (Class D)	Ordinary Structures

The prototype buildings presented herein were constructed as 6 story steel frame structures with perimeter moment-resisting CBFs to sustainably withstand lateral loads (e.g., wind and earthquake loads). They were designed under essentially regular condition without in-plane torsional effect, owing to symmetrical plan with masses and stiffnesses uniformly distributed. A plan view of 6 story square buildings with five 9.15 m bays is described in Figure 3a. Three braced frame bays denoted as the dashed lines in the figure were installed on each side. The moment-resisting frames described as the thick lines in the plan view were built with fully restrained-welded beam-to-column connections while the inside gravity load-resisting frames were built with simple pinned connections only withstanding shear force. The elevation view of the perimeter moment-resisting frame is shown in Figure 3b. Two story X-braced frame systems were accepted for frame design among various types of CBF systems. All of the CBF buildings have 3.96m story height. Column sections were designed with the uniform sizes throughout all stories while beam sections assigned to the higher stories were designed with smaller beam sizes (*i.e.*, W18x50 beam size). The details for assigning member sizes to frame design are summarized in Table 3.

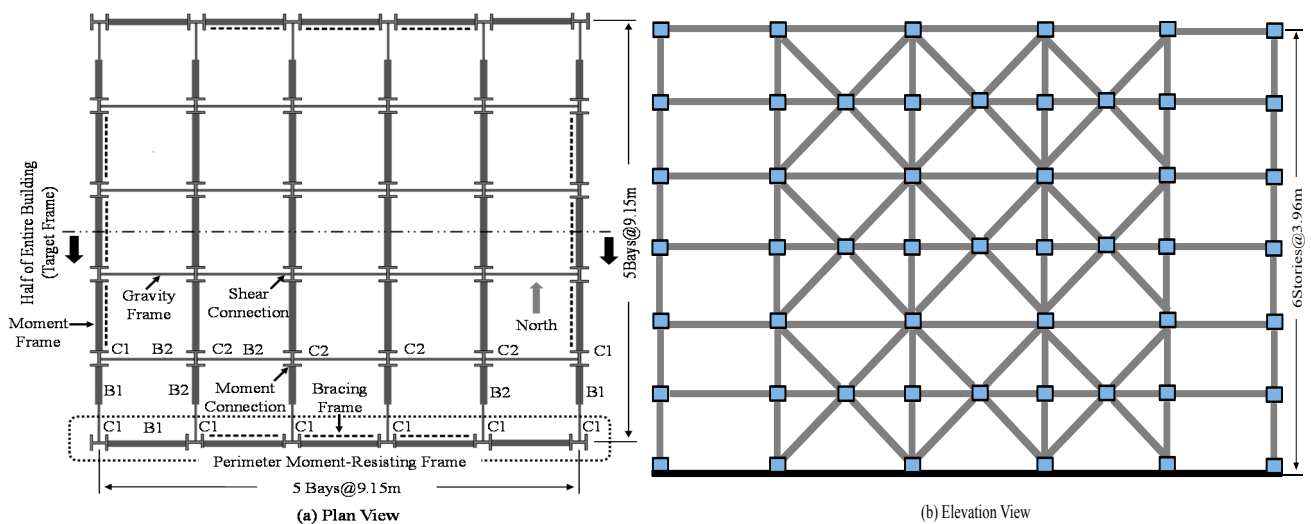


Figure 3. Design of six story braced frame buildings.

Table 3. Member sizes for prototype braced frame buildings.

Story	Column * (C1)	Beam * (B1)	CBF **	Internal Column * (C2)	Internal Beam* (B2)
1	W14x109	W24x84	HSS6x6x3/8	W12x87	W24x68
2	W14x109	W24x84	HSS6x6x3/8	W12x87	W24x68
3	W14x109	W24x68	HSS6x6x3/8	W12x87	W24x68
4	W14x109	W24x68	HSS6x6x3/8	W12x87	W24x68
5	W14x109	W18x50	HSS6x6x1/4	W12x87	W24x68
6	W14x109	W18x50	HSS6x6x1/4	W12x87	W24x68

* Gr.50 Carbon Steel; ** Gr.B Carbon Steel for Rectangular Shape; CBF: concentrically brace frame.

4. Analytical Modeling

The analytical spring models mostly used for simulating the behavior of LRB isolator devices are constructed with the OpenSEES program with an intention to perform nonlinear dynamic time-history analyses [25]. The modeling attributes are illustrated in Figure 4. The main part of the LRB isolator (*i.e.*, elastomeric rubber and lead core) was modeled as the zero-length nonlinear component spring while the cover plate was modeled as the rigid element (see Figure 4a). The behavior of the LRB isolator can be ideally characterized by the bi-linear stiffness model using three key parameters such as initial stiffness (K_e), yield force (F_1), and post-yield stiffness (K_p) (see Figures 2 and 4b), and simply simulated by using isotropic hardening material command provided in the OpenSEES program. It was assigned to the component spring element for the purpose of reproducing the force-displacement response curve. The analytical component spring models classified herein as LRB1 and LRB2 were installed on the base-isolated frame model (see Figure 5). Each LRB spring model includes the force-displacement response presented in Figure 2. The column bases of as-built frame model without base isolation are considered to be fixed. Accordingly, LRB-isolated frame models (*i.e.*, LRB1 and LRB2 models) have flexible end boundary conditions while as-built frame models possess fixed end boundary conditions.

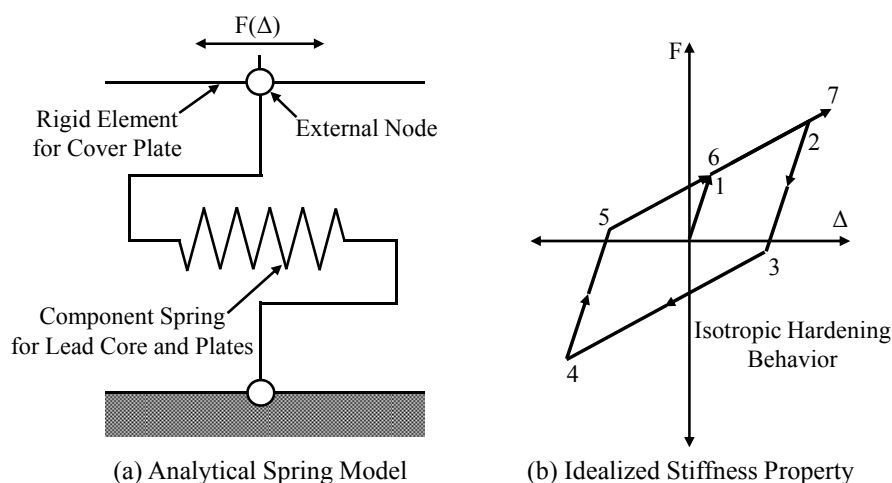


Figure 4. Analytical modeling attributes for component spring and its behavioral property.

The modeling attributes for prototype frame buildings are shown in Figure 5. All building models are symmetrical to their center axes with uniform mass and stiffness distribution, and thus can be modelled as 2D frame models. The 2D frame models consisting of perimeter moment-resisting frames and gravity

load-resisting frames were used for nonlinear dynamic time-history analyses with several NF ground motions. The beam and column members in the moment-resisting frame were modeled as nonlinear beam-column elements with 2D fiber sections aiming to reproduce inelastic behavior. P-delta coordinate transformations incorporating to these nonlinear elements were taken into consideration for simulating geometric nonlinearity involving with second-order large deformation. The welded-type moment connections between beam and column as well as the stiffening gusset plates were constructed with the rigid offsets assigned to the beam members. The leaning column members in the interior gravity load-resisting frames are required to withstand half of entire building weight. These leaning columns were modeled as elastic beam-column elements with geometric section properties (e.g., cross-section area, second moment of inertia, and torsional moment of inertia), and mainly subjected to dead plus live loads. The rigid links replaced for concrete slabs or diaphragm constraints were equipped between perimeter frames and interior frames so that each floor should translate as a rigid body. All steel members were fabricated with Gr. 50 steel containing 1.5% strain hardening ratio. The transient equilibrium method suggested by Newmark [26] was used to perform the nonlinear dynamic time-history analyses. According to common practice for code designed steel structures [27,28], an effective viscous damping coefficient of 5% was applied to the analytical frame models. The effective damping can be generated by using the Rayleigh command provided in the OpenSEES program. The point masses composed of dead loads plus 0.2 times live loads were assigned to individual nodes in order to generate shear forces resulting from ground acceleration. The resulting data such as shear forces and displacements were collected by using the recorder command.

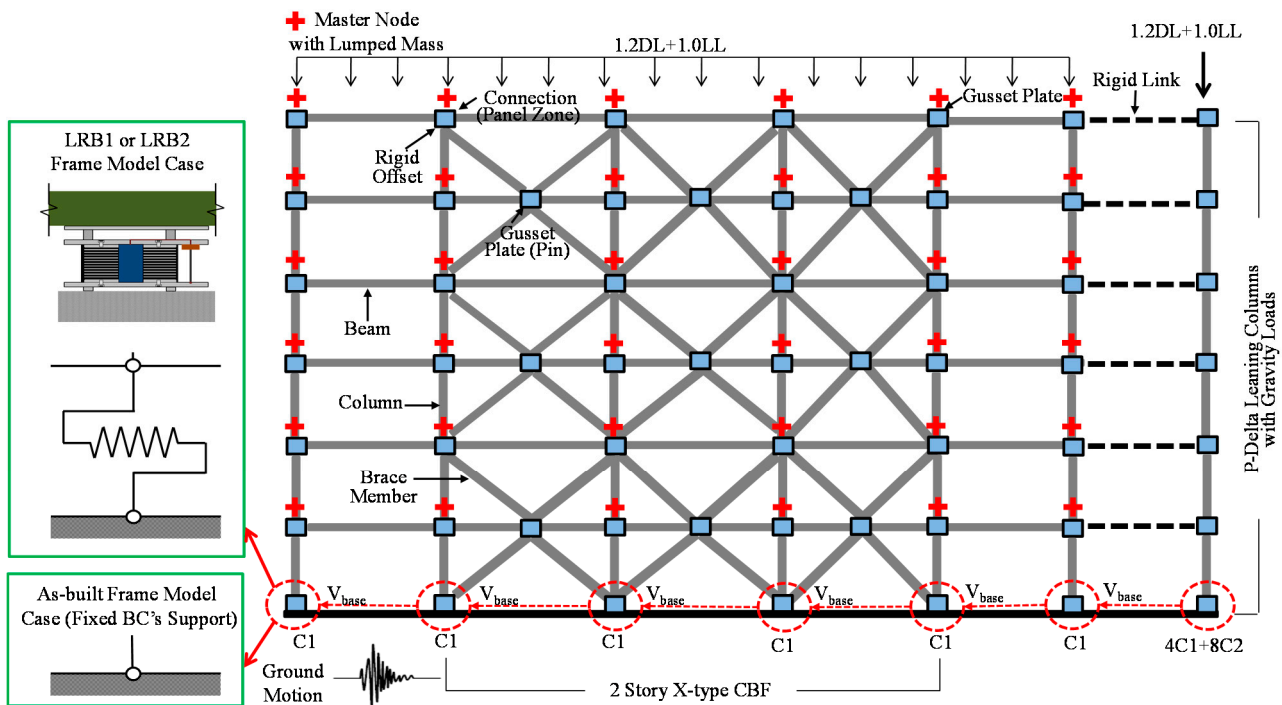


Figure 5. Modeling attributes for 2D frame models.

The brace members were also modeled as nonlinear beam-column elements with 2D fiber sections. The modeling of the brace members is shown in Figure 6. The discrete fiber sections that contain nonlinear material behavior can configure the cross-section of the hollow steel tube. The section

properties were assigned to the integration points distributed over the nonlinear beam-column element. The brace members were connected to other members as pinned connections because they were considered to be structural elements only subjected to axial forces. For this reason, the brace member with the hollow tube section is susceptible to buckling in compression. The initial imperfection generated by offsetting the node on the middle of the brace member may be required to reproduce buckling failure in the frame model. The brace member under compression behaves as elastic until it reaches the buckling state (P_{cr}). Global buckling that indicates the peak load suddenly occurs at the middle of the brace member prior to the compressive yielding of the brace member. Moreover, other characteristic branches concerning negative stiffness after post-buckling, unloading, elastic tension reloading, and uniaxial tensile yielding (P_y) are also found at the hysteretic behavior curve (see Figure 6b).

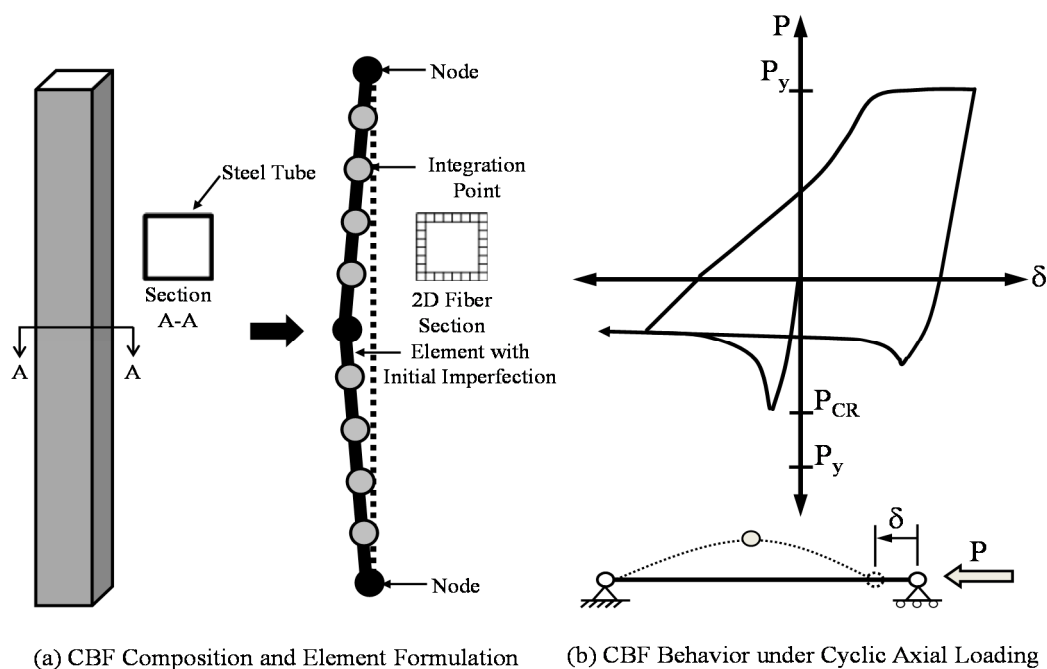


Figure 6. Modeling of the brace members.

5. Near-Fault Ground Motions

The ground motion data based on historic earthquake records were developed as a part of the FEMA/SAC project [29]. A set of 20 ground motion time histories (10 two-components) were selected to represent near-fault (NF) ground motions from earthquakes possessing a variety of faulting mechanisms (e.g., strike, rupture, oblique, and thrust) in the magnitude of 6.7 to 7.4 on the Richter scale (see Table 4). The individual components of each ground motion couple were rotated with 45 degrees away from fault-normal and fault-parallel orientations. The closest distances to reach shall crustal faults are ranged from 0 to 10 km, and the closest distances for blind thrust faults are ranged from 6 to 18 km [30,31]. These magnitudes and distance ranges govern the UBC Seismic Hazard Zone 4 for return periods of 10% in 50 years [29–31]. Detailed information on the NF ground motions used in the analyses is given to Table 4 with the variability of magnitude, distance from the epicenter, and duration time. All of NF ground motions presented herein have been derived from historical earthquake recordings. The maximum and minimum peak ground accelerations (PGAs) are also given to this table. Owing to the

variability of NF ground motions used herein, statistical investigations with respects to base shear forces and inter-story drifts for individual model cases are conducted after observing the analysis results.

Table 4. Near-fault ground motion data used for nonlinear dynamic analyses (PGA: peak ground acceleration).

Ground Motion ID	Earthquake Record	Richter Scale	Distance (km)	Duration (sec)	Max. PGA (g)	Min. PGA (g)
NF01	1978 Tabes	7.4	1.2	50	0.90	−0.86
NF02	1979 Tabes	7.4	1.2	50	0.98	−0.75
NF03	1989 Loma Prieta (Los Gatos)	7	3.5	25	0.72	−0.64
NF04	1989 Loma Prieta (Los Gatos)	7	3.5	25	0.46	−0.44
NF05	1989 Loma Prieta (Lex Dam)	7	6.3	40	0.59	−0.69
NF06	1989 Loma Prieta (Lex Dam)	7	6.3	40	0.37	−0.28
NF07	1992 Mendocino	7.1	8.5	60	0.64	−0.62
NF08	1992 Mendocino	7.1	8.5	60	0.60	−0.66
NF09	1992 Erzincan	6.7	2.0	21	0.43	−0.31
NF10	1992 Erzincan	6.7	2.0	21	0.46	−0.27
NF11	1992 Landers	7.3	1.1	50	0.71	−0.71
NF12	1992 Landers	7.3	1.1	50	0.61	−0.80
NF13	1994 Northridge (Rinaldi)	6.7	7.5	15	0.62	−0.89
NF14	1994 Northridge (Rinaldi)	6.7	7.5	15	0.38	−0.39
NF15	1994 Northridge (Olive View)	6.7	6.4	60	0.51	−0.73
NF16	1994 Northridge (Olive View)	6.7	6.4	60	0.60	−0.56
NF17	1995 Kobe	6.9	3.4	60	1.09	−0.73
NF18	1995 Kobe	6.9	3.4	60	0.58	−0.57
NF19	1995 Kobe (Takatori)	6.9	4.3	40	0.79	−0.51
NF20	1995 Kobe (Takatori)	6.9	4.3	40	0.38	−0.42

Figure 7 shows 5% damped spectral accelerations (S_g) for individual NF ground motions according as the fundamental time period of the structure (T) increases. The mean (or average) spectral acceleration for 20 NF ground motions with 1.0 scale factors (SF) is also plotted as the red line in this figure. The base shear forces required for seismic design are easily estimated by utilizing these response spectra since the structures are assumed to behave as single degree of freedom (SDOF) systems subjected to independent earthquake ground motions. The OpenSEES program can provide the computational command to estimate the fundamental time periods of the LRB frame models, which have an influence on the initial stiffness of the used LRB isolator devices, including those of the as-built frame models. On finding out the fundamental time period of the relevant structure, the peak response of the structure can be estimated by reading the acceleration value from the response spectrum curve for appropriate natural frequency or fundamental time period. The mean response spectral acceleration for the as-built frame model was taken as approximately 1.38 g for 0.8 s fundamental time period while that for the LRB-isolated frame model (*i.e.*, LRB1 frame model) was taken as 0.89 g for 1.35 s one (see Figure 7). The LRB isolators extend the fundamental time period of the structure away from the high band of the spectral acceleration, meaning that they contribute effectually toward reducing seismic shear forces converted

from ground accelerations. The response spectral accelerations for individual NF ground motion data according to each model case are presented in Figure 8. The limits of the mean response spectral accelerations for individual model cases (*i.e.*, 1.38 g, 0.94 g, and 0.89 g for As-built, LRB2, and LRB1 frame model, respectively) are also plotted as dashed lines in the figure.

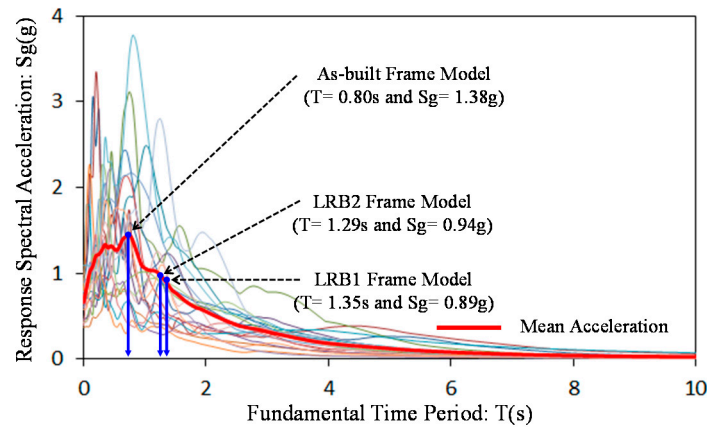


Figure 7. 5% damped spectral accelerations for near-fault ground motions (scale factor (SF) = 1.0) and fundamental time periods for individual model cases.

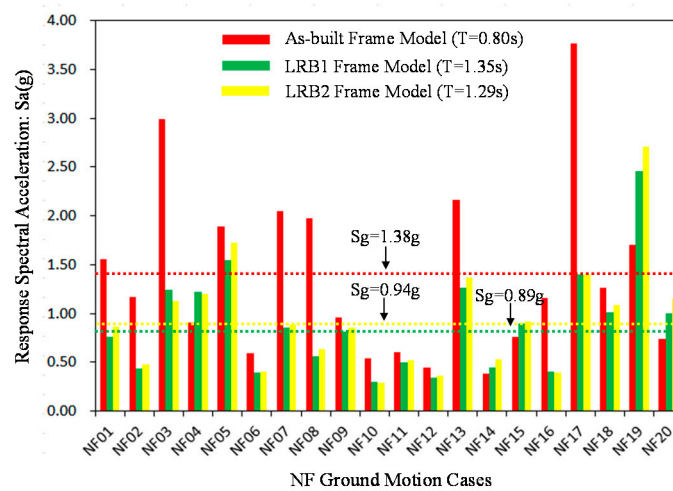


Figure 8. Response spectral accelerations for individual ground motion data according to each model case.

6. Seismic Responses

The nonlinear dynamic time-history analyses were performed on 2D frame models with 20 NF ground motion data mentioned above in an attempt to check the efficacy of LRB isolation systems in the frame building. The seismic responses of the LRB-isolated frame models were compared to those of the as-built frame model in terms of roof displacements, base shear forces, and inter-story drifts. The resulting curves from time-history analyses performed with representative NF08 ground motion data are presented as compared to each frame model in Figures 9–11.

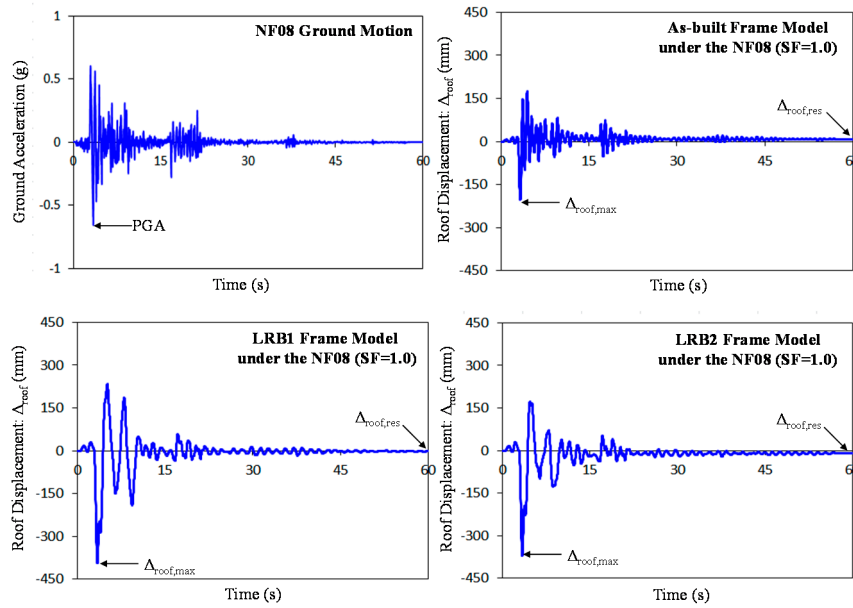


Figure 9. Nonlinear dynamic analysis results (time vs. roof displacement curves).

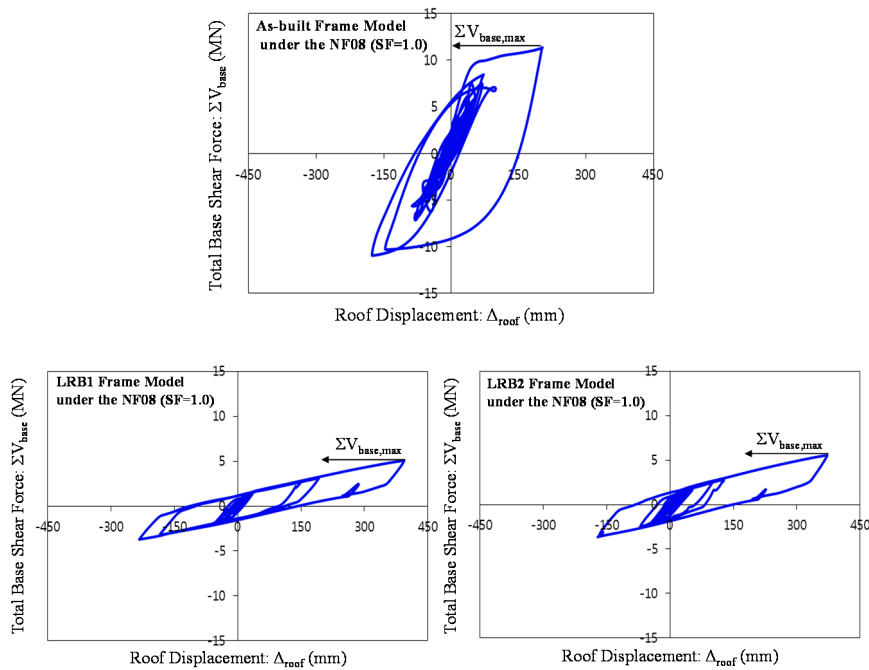


Figure 10. Nonlinear dynamic analysis results (roof displacement vs. total base shear force curves).

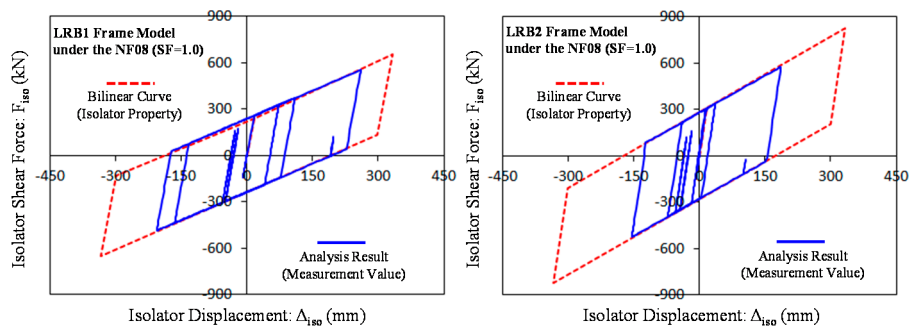


Figure 11. Displacement vs. shear force curves measured at the exterior column-base isolator.

The NF08 ground motion has a relatively long duration time (60 s) with 0.66 g peak ground acceleration (PGA). The time *versus* roof displacement curves presented in Figure 9 are obtained after conducting time-history analyses on three comparative frame models subjected to this ground motion. The LRB-isolated frame models show larger maximum roof displacements than the as-built frame model without base isolation because they are equipped with flexible end boundary conditions. The maximum roof displacements for the LRB1 and LRB2 frame model under the NF08 ground motion with 1.0 scale factor are approximately 400 mm and 390 mm, respectively. On the other hand, the maximum roof displacement of the as-built frame model is approximately 200 mm, indicating almost half of the maximum roof displacements of the LRB-isolated frame models. The generation times of maximum roof displacements are almost same for each frame model, and commonly follow PGA time by about 1 s. As compared to the as-built frame model, both larger amplitudes and more vibrations are displayed in the LRB-isolated frame models with relatively longer fundamental time periods.

For another analysis results, the roof displacement *versus* total base shear force curves are presented in Figure 10. The total base shear forces are obtained by summing up all reaction forces measured at the column bases. The LRB-isolated frame models exhibit smaller total base shear forces than the as-built frame model regardless of having much larger maximum roof displacement. Overall, the maximum total base shear forces of the as-built frame model, which is two times greater than those of the LRB-isolated frame models, are delivered into the superstructure. Therefore, LRB isolator devices acting as laterally flexible stiffnesses equipped on boundaries between superstructures and substructures alleviate structural damage effectually as reducing the generation of base shear forces changed from ground accelerations. As shown in the figures, the force-displacement responses of the LRB-isolated frame models can be characterized as bilinear hysteresis loops similar to the behavior of the typical LRB isolator. It indicates that the behavior of the entire building is considerably affected by the mechanical property of the used base isolation system. The LRB2 frame model has slightly larger maximum total base shear force than the LRB1 frame model on the ground of inherent characteristics for the LRB isolator devices used. The isolator displacement *versus* shear force curves measured at the exterior column-base isolator (see C1 position of Figure 5) are also investigated to verify adequacy for the analytical modeling of the base isolation system. As shown in Figure 11, the bilinear approximation curves plotted based on isolator properties (dashed red lines) have good agreements with the measured analytical results (solid blue lines) in terms of initial stiffness, yield force, post-yield stiffness, and force at the specific point.

7. Statistical Investigations

The statistical investigations into seismic responses were conducted based on the results of several time-history analyses for the purpose of reliably accessing not only seismic performance but also the extent of structural damage. The statistical investigations of the maximum roof displacements ($\Delta_{\text{roof,max}}$) for individual frame models according to increasing scale factors are illustrated in Figure 12. The statistical lines indicating 15.9th, 50.0th (or median), and 84.1th percentile ranks are drawn in the graphs together with individual resulting data points obtained from all analysis results. As the scale factor of the ground motion increases at a fixed rate, the statistical lines for the values of the maximum roof displacements gradually ascend in the straight curves. The ranges of data scatter increase as well. The

LRB-isolated frame models that permit base movements in the direction of the ground motion show larger statistical values than the as-built frame model. Furthermore, the LRB1 model has slightly higher statistical percentile lines (approximately 5%) than the LRB2 model owing to more flexible LRB properties.

For another investigation variables, maximum total base shear forces ($\Sigma V_{base,max}$) for individual frame models according to increasing scale factors are presented in Figure 13. The statistical values for the maximum total base shear forces are commonly proportional to the scale factors of the ground motions increasing as well. As expected, the as-built frame model is susceptible to higher base shear forces in comparison of other LRB-isolated frame models. When examining the distribution of the total base shear forces at the graphs, it can be found that the LRB base isolators lead the generation of the base shear force to alleviate considerably.

After earthquake events, a statistical inquiry into the distribution of the residual roof displacements is required to figure out the extent of structural damage generated by the transmitted base shear forces. The statistical investigations of the residual roof displacements ($\Delta_{roof,res}$) for individual frame models according to increasing scale factors are presented in Figure 14. The severe failures representing over 80mm residual roof displacements are mostly displayed at the graphs of the as-built frame model case, and generated even under the ground motions with the value of 0.6 scale factor. Therefore, the upper statistical percentile lines (50.0th and especially 84.1th percentile) for the distribution of the residual roof displacements ascend rapidly at the as-built frame model as increasing the scale factors of the ground motions. In contrast, the statistical lines of the LRB-isolated frame models show gentle ascent at the graphs of the residual roof displacements according to the increasing scale factors, meaning that these isolated frame models are little susceptible to structural damage even under strong ground motions. As compared to each frame model, the statistical values for maximum roof displacements, maximum total base shear forces, and residual roof displacements are finally summarized in Table 5. The values of each mean and standard deviation (SD) are also presented in this table.

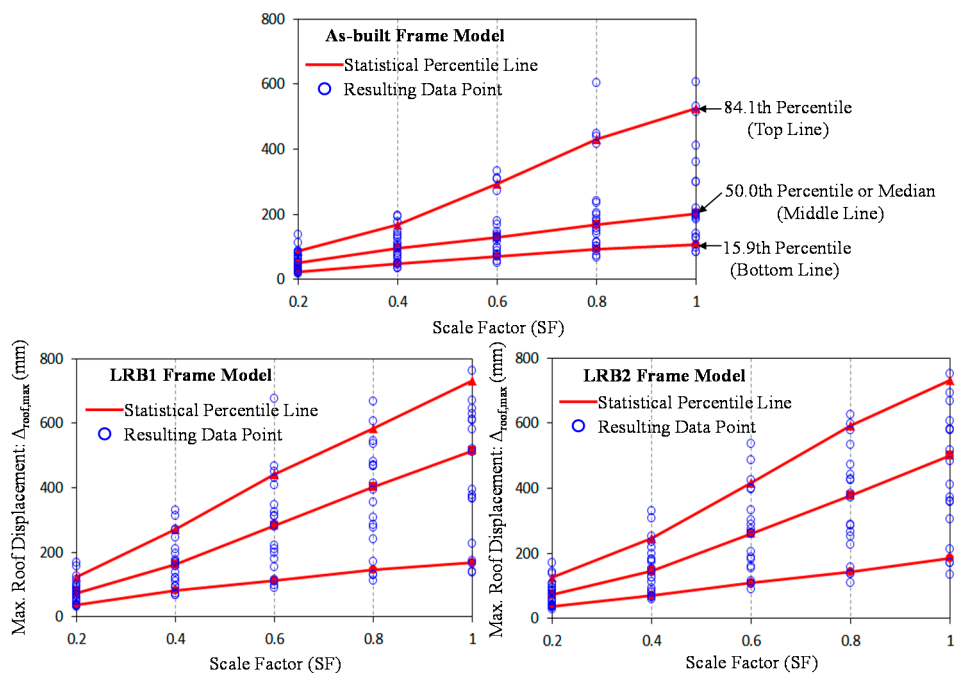


Figure 12. Statistical investigations of the maximum roof displacements ($\Delta_{roof,max}$) for individual frame models according to increasing scale factors.

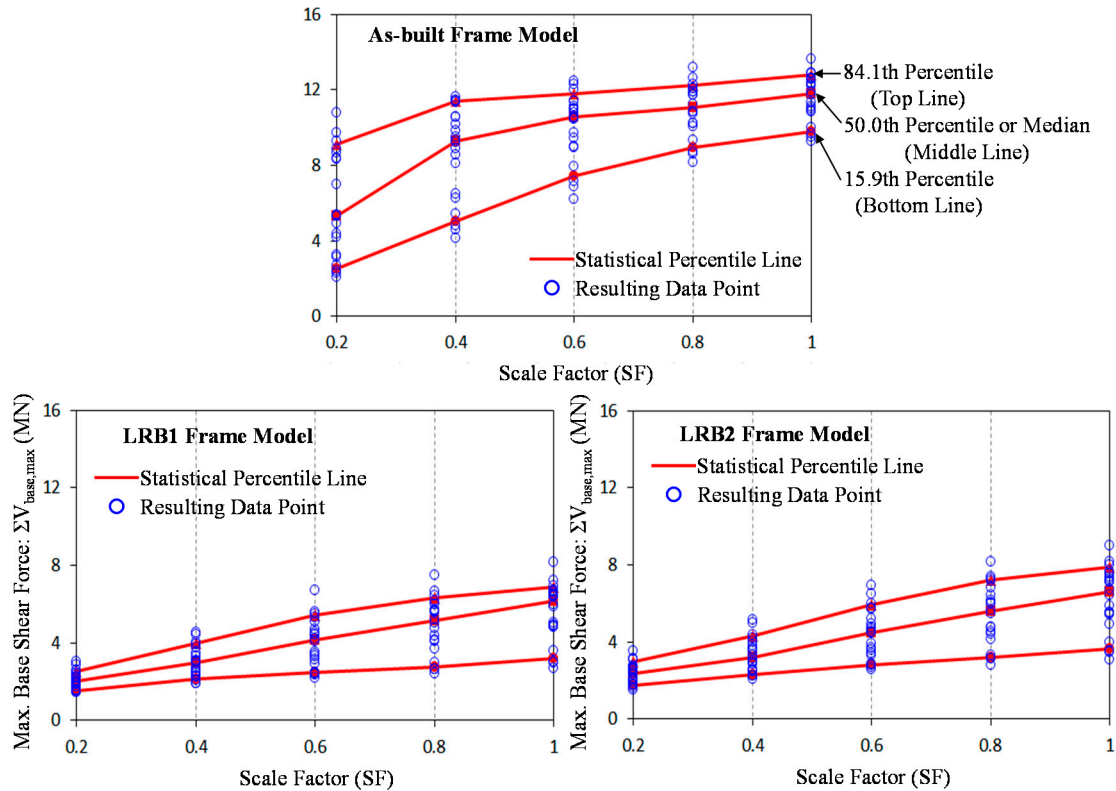


Figure 13. Statistical investigations of the maximum total base shear forces ($\Sigma V_{base,max}$) for individual frame models according to increasing scale factors.

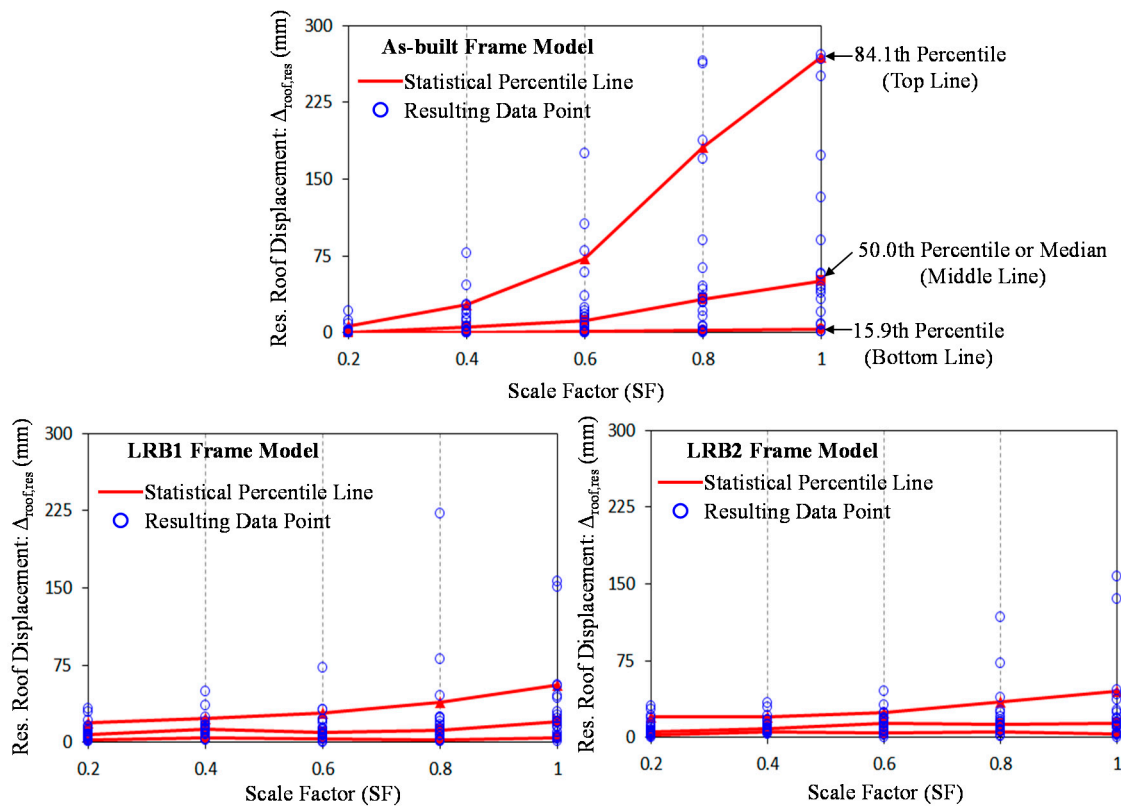


Figure 14. Statistical investigations of the residual roof displacements ($\Delta_{roof,res}$) for individual frame models according to increasing scale factors.

Table 5. Comparison and summary of the statistical valises for maximum roof displacements, maximum total base shear forces, and residual roof displacements.

Evaluation Item	Model ID	SF = 0.2					SF = 0.4					SF = 0.6					SF = 0.8					SF = 1.0				
		15.9%	50.0%	84.1%	Mean	SD	15.9%	50.0%	84.1%	Mean	SD	15.9%	50.0%	84.1%	Mean	SD	15.9%	50.0%	84.1%	Mean	SD	15.9%	50.0%	84.1%	Mean	SD
$\Delta_{\text{roof,max}}$ (mm)	As-Built	23.7	50.3	86.8	56.6	32.2	47.4	96.4	166.9	101.2	49.4	71.0	127.6	294.8	148.2	86.1	91.8	167.7	430.7	212.4	144.5	107.0	200.6	524.4	287.9	204.3
	LRB1	35.6	72.7	122.6	77.8	38.9	80.2	162.1	270.7	169.4	79.5	112.0	281.9	442.6	283.4	147.4	144.8	403.6	584.6	400.2	202.5	168.2	515.3	731.2	508.7	295.6
	LRB2	38.0	73.8	126.5	77.4	38.9	71.2	146.1	245.9	159.2	77.5	109.3	261.1	416.1	263.4	129.0	144.1	377.1	591.0	376.8	186.6	185.4	500.3	731.1	503.9	267.1
$\Sigma V_{\text{base,max}}$ (MN)	As-Built	2.5	5.3	9.1	5.8	2.8	5.0	9.3	11.4	8.6	2.4	7.4	10.5	11.8	10.0	1.8	8.9	11.0	12.2	10.9	1.4	9.8	11.8	12.8	11.6	1.2
	LRB1	1.5	2.0	2.5	2.0	0.4	2.1	3.0	4.0	3.0	0.8	2.4	4.1	5.4	4.0	1.2	2.8	5.1	6.3	4.9	1.4	3.2	6.2	6.9	5.6	1.5
	LRB2	1.8	2.3	3.0	2.3	0.5	2.3	3.2	4.3	3.3	0.9	2.8	4.5	5.9	4.4	1.3	3.2	5.6	7.2	5.4	1.5	3.7	6.6	7.9	6.2	1.7
$\Delta_{\text{roof,res}}$ (mm)	As-Built	0.3	0.6	6.4	2.8	5.1	0.4	5.5	26.9	13.4	19.0	0.8	12.1	72.7	29.1	43.5	1.8	32.2	181.7	65.5	83.2	3.5	50.6	269.6	117.2	137.4
	LRB1	2.5	7.2	19.3	10.2	8.6	4.8	12.8	23.2	14.9	10.9	3.3	9.2	28.6	14.8	16.1	2.0	11.9	38.5	27.0	48.3	4.5	19.8	55.6	35.3	42.6
	LRB2	2.4	6.0	20.5	9.6	8.4	5.6	9.0	20.0	12.4	8.1	4.0	13.6	24.0	14.6	10.7	5.6	13.1	34.6	21.7	26.7	2.9	14.3	45.3	29.6	41.0

In the frame, the responses of the LRB base isolators are also investigated through the nonlinear dynamic time-history analyses. The necessary data were collected by measuring forces and displacements at the exterior column base isolator. According to increasing scale factors, maximum isolator displacements for individual LRB-isolated frame models ($\Delta_{iso,max}$) are presented in Figure 15. The LRB1 frame model presents a similar ascent slope pattern as the LRB2 frame model on the occasion of increasing scale factors, but has larger statistical values owing to more flexible behavior displayed at the LRB isolator. The ranges of data scatter indicating the degree of uncertainty are determined by the value of standard deviations. At every scale factors, larger mean values and standard deviations are found at the LRB1 frame model.

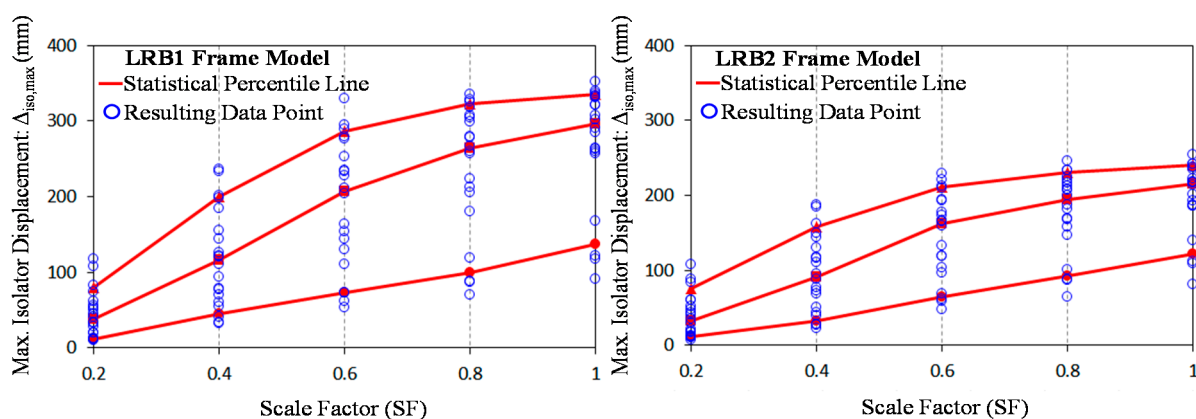


Figure 15. Statistical investigations of the maximum isolator displacements ($\Delta_{iso,max}$) for individual LRB-isolated frame models according to increasing scale factors.

As shown in Figure 16, residual isolator displacements ($\Delta_{iso,res}$) are also presented for the purpose of conducting more statistical investigations required to make sure the performance of the LRB isolators in the frame building. After checking residual roof displacements presented in Figure 14, it can be affirmed that there is a little difference to corresponding residual isolator displacements. This implies that most of relative residual displacements occur at the base isolation system.

In addition to isolation function, it is important to check energy dissipation capacity in the single base isolator during NF ground motions. The statistical investigations of the maximum isolator energies ($E_{iso,max}$) for individual LRB-isolated frame models according to increasing scale factors are presented in Figure 17. When the isolation system is fully excited by each of the NF ground motions, dissipated energy corresponds to the area of the hysteresis force-displacement loop as given to Figure 11. As expected, the graphs of the maximum isolator energies show a totally similar pattern as those of the maximum isolator displacements, including the distributional trends of data scatter. As compared to each LRB-isolated frame model, the statistical values for the maximum isolator displacements, residual isolator displacements, and maximum dissipated isolator energies are summarized in Table 6. Similarly, this table also presents the values of each mean and standard deviation (SD).

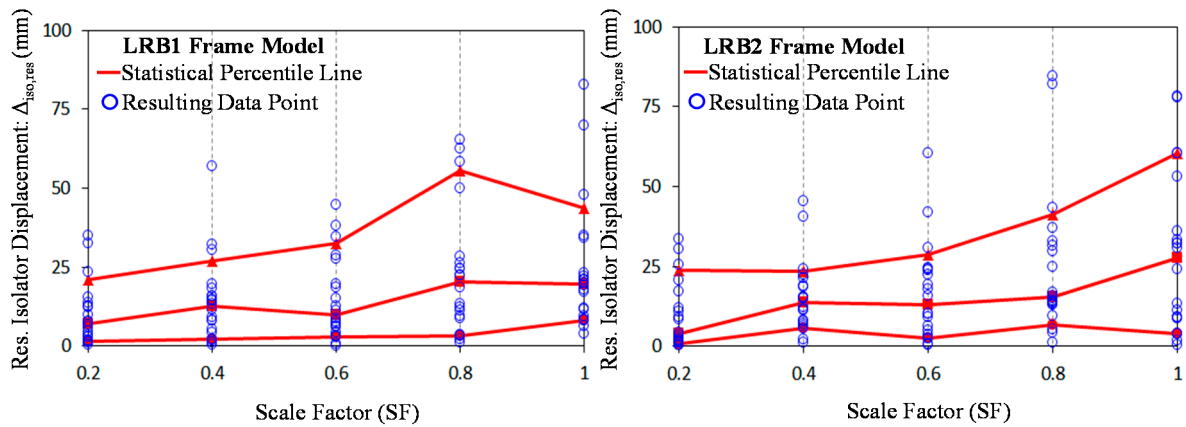


Figure 16. Statistical investigations of the residual isolator displacements ($\Delta_{iso,res}$) for individual LRB-isolated frame models according to increasing scale factors.

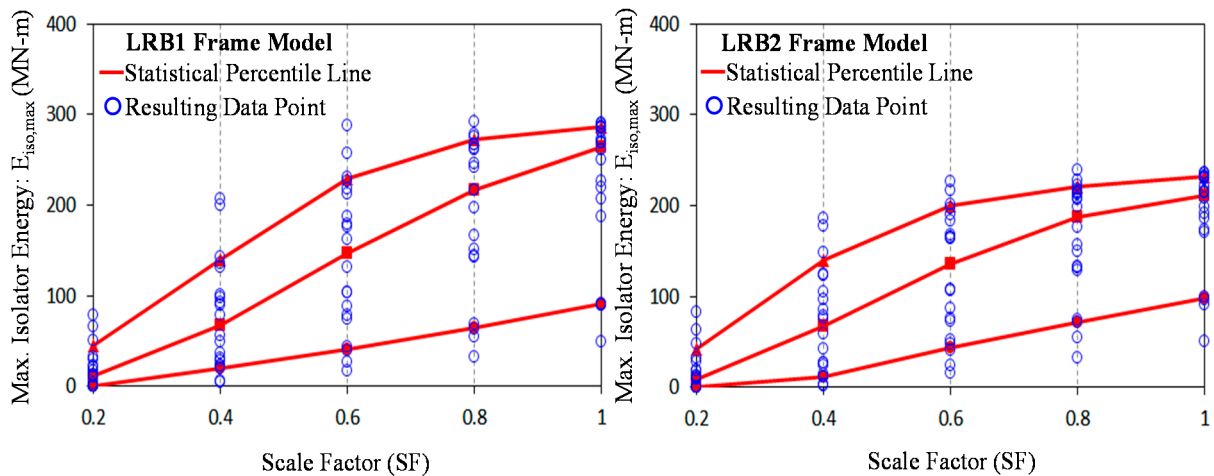


Figure 17. Statistical investigations of the maximum isolator energies ($E_{iso,max}$) for individual LRB-isolated frame models according to increasing scale factors.

According to the availability of base isolation implementation, seismic performance and structural damage for individual 6 story frame models subjected to NF ground motions can be evaluated through the observation of maximum inter-story drifts and residual inter-story drifts after nonlinear dynamic time-history analyses. The allowable maximum inter-story drift limits (generally taken as 2%) stipulated in the ASCE7-05 design code are plotted as the dashed lines in Figure 18. Two residual inter-story drift limits required for either economical rehabilitation or completely collapse decision (0.5% or 1.0% limit) are also plotted as the dashed lines in Figure 19. Some scientists suggest that if the residual inter-story drifts are greater than 0.5%, from an economic point of view, building owners had better rebuild the entire structure rather than repair only damaged parts [32]. Although the frame building undergoes residual inter-story drifts smaller than 0.5%, extra repair costs are indeed required to recover the laterally deformed structure to its original state one. Above all, building residents feel severe dizziness and nausea as the residual inter-story drift level begins to be over 1.0%. It represents the total loss of the frame building.

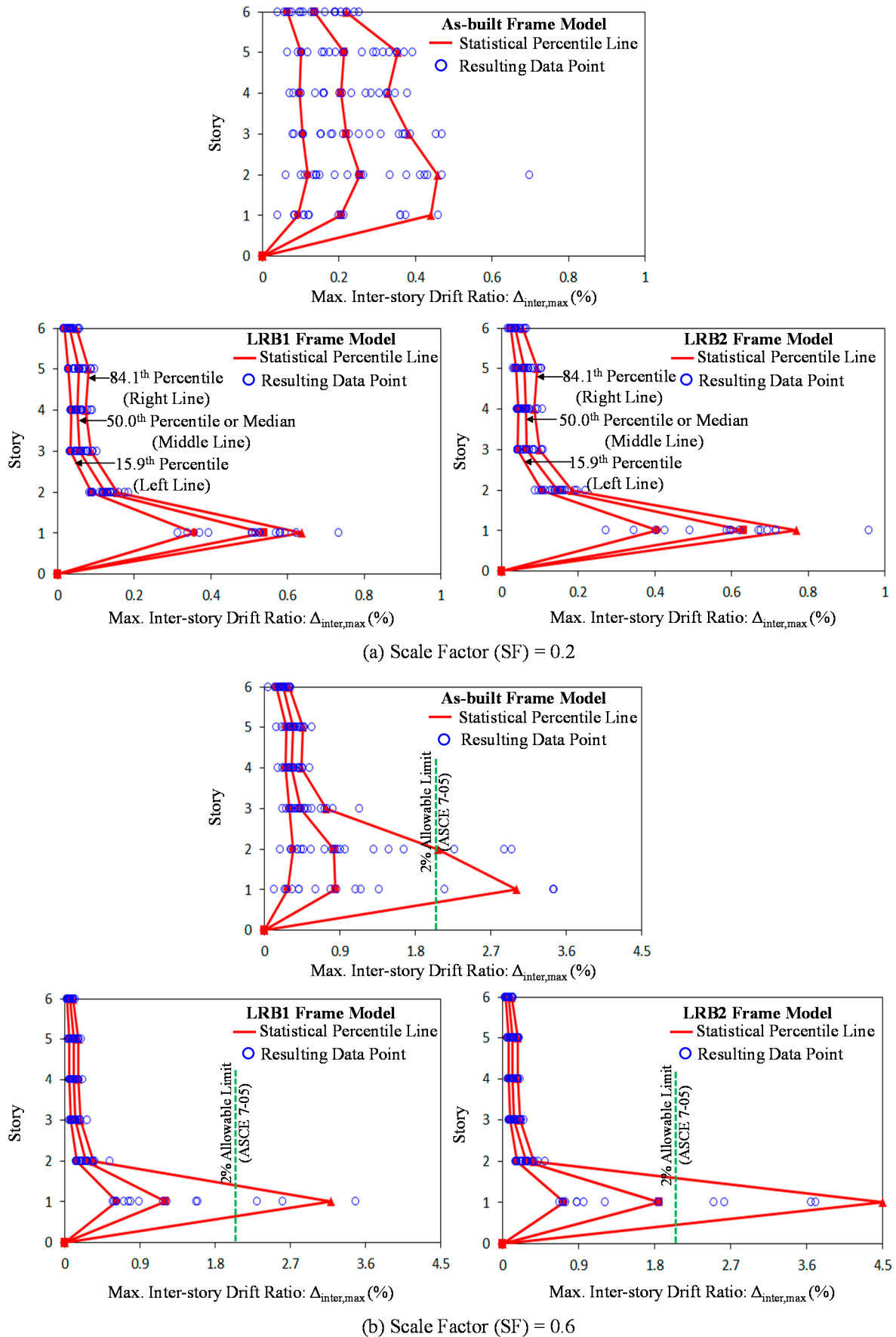
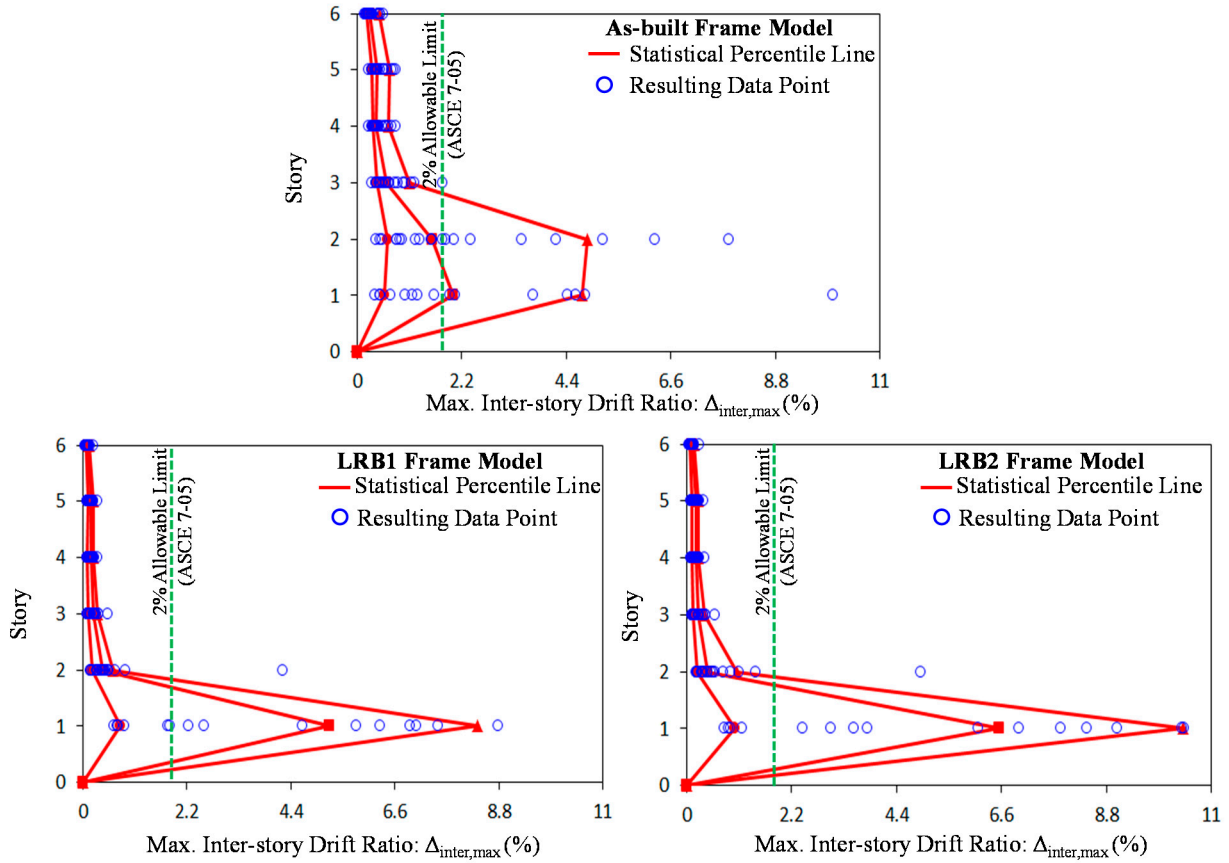
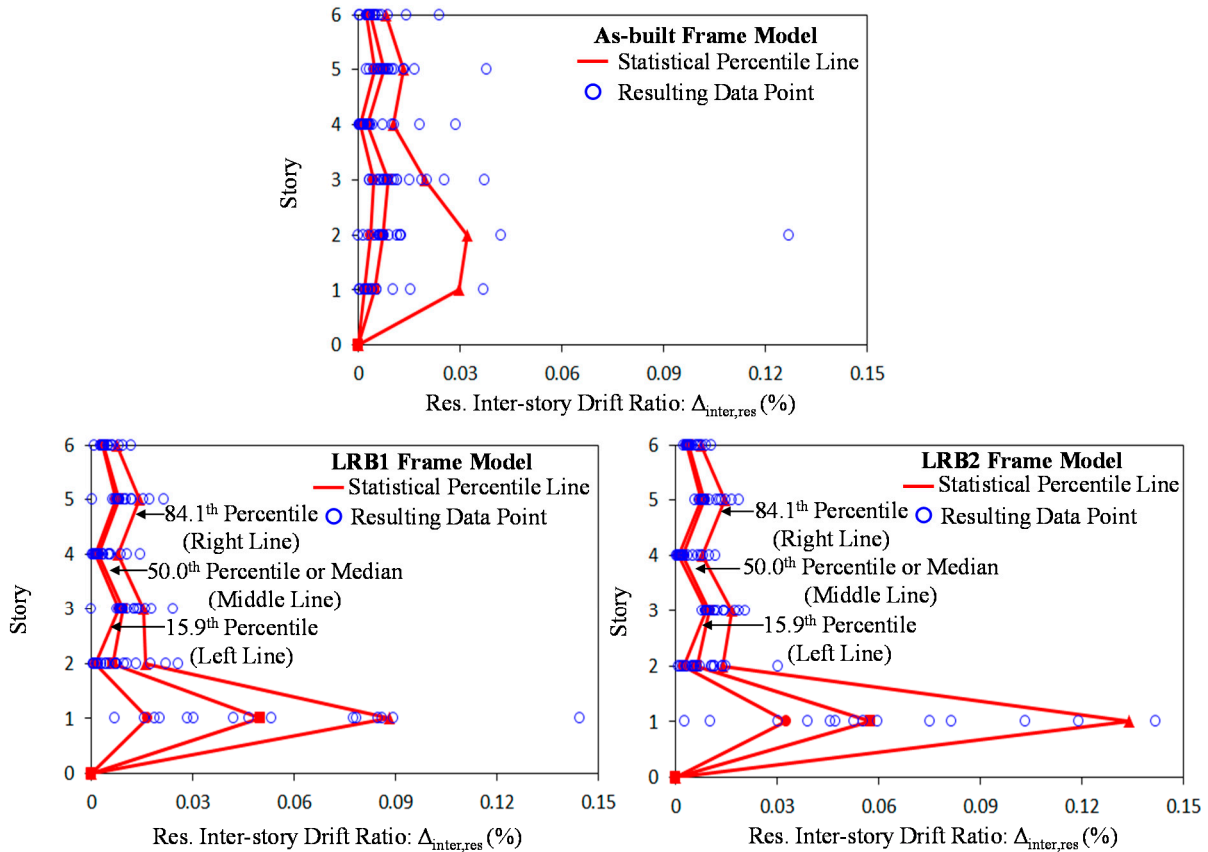


Figure 18. Statistical investigations of the maximum inter-story drift ratios ($\Delta_{inter,max}$) for individual frame models under SF = 0.2, 0.6, and 1.0, respectively.



(c) Scale Factor (SF) = 1.0



(a) Scale Factor (SF) = 0.2

Figure 19. Cont.

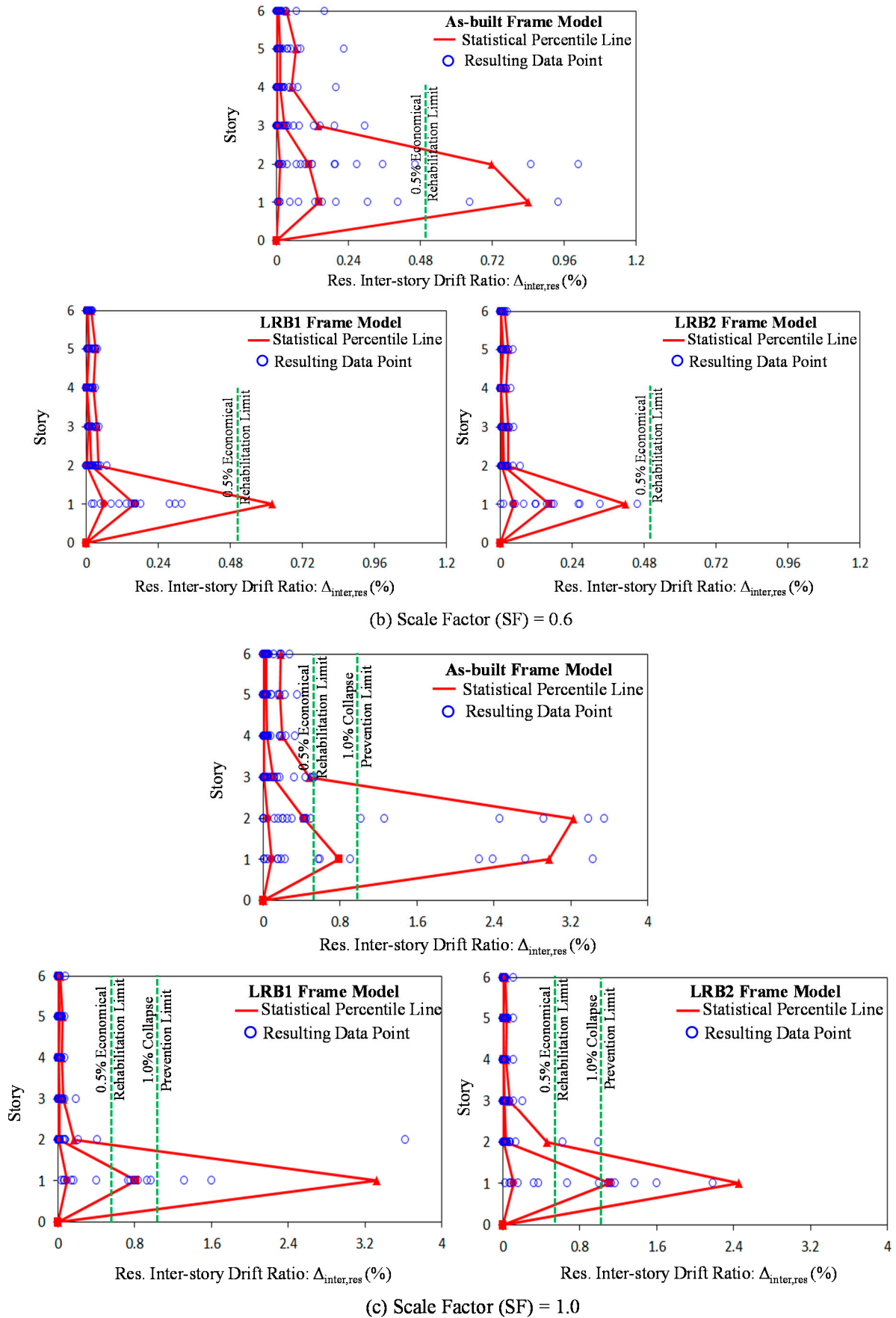


Figure 19. Statistical investigations of the residual inter-story drift ratios ($\Delta_{inter,res}$) for individual frame models under SF = 0.2, 0.6, and 1.0, respectively.

Table 6. Comparison and summary of the statistical values for maximum isolator displacements, residual isolator displacements, and dissipated energies.

Evaluation Item	Model ID	SF = 0.2					SF = 0.4					SF = 0.6					SF = 0.8					SF = 1.0				
		15.9%	50.0%	84.1%	Mean	SD	15.9%	50.0%	84.1%	Mean	SD	15.9%	50.0%	84.1%	Mean	SD	15.9%	50.0%	84.1%	Mean	SD	15.9%	50.0%	84.1%	Mean	SD
$\Delta_{iso,max}$ (mm)	LRB1	11.7	37.4	79.6	44.0	31.1	45.2	115.5	200.1	118.5	63.7	73.3	207.5	286.1	190.0	84.3	98.9	263.4	322.9	237.3	84.4	137.4	295.9	335.8	269.6	78.7
	LRB2	11.1	32.7	76.0	38.6	28.8	32.1	91.7	157.9	95.8	51.2	64.1	162.5	211.5	145.4	56.8	91.8	193.7	230.6	177.6	53.3	121.2	214.7	239.9	196.4	47.9
$\Delta_{iso,res}$ (mm)	LRB1	1.6	7.1	20.8	10.1	9.7	2.0	12.5	26.9	14.2	13.1	2.9	10.0	32.6	14.9	12.9	3.3	20.4	55.5	23.4	19.8	8.3	19.7	43.5	24.6	20.3
	LRB2	0.7	3.9	23.8	9.3	10.3	5.8	13.6	23.5	15.5	11.2	2.5	12.9	28.6	16.5	14.9	6.8	15.4	41.2	25.1	22.2	3.8	27.5	60.5	29.0	24.6
$E_{iso,max}$ (MN-m)	LRB1	0.0	11.0	44.7	17.8	22.6	20.3	67.4	140.4	77.5	59.6	41.1	146.6	229.3	142.2	80.3	64.7	216.2	272.8	192.1	82.4	90.7	264.6	286.9	224.4	77.9
	LRB2	0.0	9.2	42.5	16.6	23.0	11.3	67.6	140.1	71.0	56.9	43.0	135.1	200.3	125.2	67.6	71.8	187.3	220.9	163.6	62.5	97.3	211.5	231.4	186.2	55.0

Table 7. Comparison and summary of the statistical values for maximum and residual inter-story drift ratios.

SF	Evaluation Item	Model ID	1st Story			2nd Story			3rd Story			4th Story			5th Story			6th Story		
			50%	Mean	SD															
0.2	$\Delta_{inter,max}$ (mm)	As-Built	0.204	0.279	0.236	0.255	0.309	0.223	0.219	0.242	0.123	0.206	0.214	0.098	0.213	0.227	0.102	0.136	0.144	0.065
		LRB1	0.538	0.524	0.115	0.125	0.125	0.028	0.058	0.061	0.021	0.050	0.055	0.016	0.055	0.055	0.020	0.032	0.033	0.012
		LRB2	0.631	0.605	0.166	0.146	0.144	0.035	0.065	0.068	0.023	0.062	0.062	0.018	0.059	0.062	0.022	0.036	0.037	0.013
	$\Delta_{inter,res}$ (mm)	As-Built	0.005	0.025	0.061	0.007	0.025	0.049	0.009	0.012	0.008	0.003	0.005	0.007	0.008	0.010	0.007	0.004	0.005	0.005
		LRB1	0.050	0.060	0.041	0.006	0.008	0.007	0.009	0.011	0.005	0.002	0.004	0.004	0.008	0.010	0.004	0.004	0.005	0.002
		LRB2	0.058	0.075	0.056	0.006	0.008	0.007	0.010	0.012	0.004	0.002	0.004	0.003	0.008	0.010	0.003	0.004	0.005	0.002
0.4	$\Delta_{inter,max}$ (mm)	As-Built	0.434	0.662	0.561	0.520	0.643	0.436	0.405	0.392	0.154	0.318	0.304	0.082	0.323	0.319	0.085	0.192	0.199	0.055
		LRB1	0.727	0.802	0.287	0.177	0.182	0.047	0.083	0.090	0.028	0.080	0.082	0.026	0.074	0.081	0.028	0.045	0.049	0.017
		LRB2	0.838	1.059	0.590	0.198	0.205	0.053	0.101	0.101	0.034	0.093	0.092	0.030	0.095	0.092	0.033	0.057	0.055	0.020
	$\Delta_{inter,res}$ (mm)	As-Built	0.030	0.149	0.227	0.031	0.115	0.153	0.017	0.034	0.044	0.010	0.016	0.023	0.010	0.020	0.029	0.007	0.012	0.019
		LRB1	0.084	0.098	0.066	0.010	0.014	0.012	0.010	0.013	0.008	0.002	0.007	0.008	0.008	0.012	0.008	0.004	0.006	0.005
		LRB2	0.117	0.153	0.122	0.009	0.013	0.010	0.009	0.012	0.007	0.002	0.005	0.006	0.008	0.011	0.007	0.004	0.005	0.004

Table 7. Cont.

SF	Evaluation Item	Model ID	1st Story			2nd Story			3rd Story			4th Story			5th Story			6th Story		
			50%	Mean	SD															
0.6	$\Delta_{inter,max}$ (mm)	As-Built	0.845	1.207	1.069	0.828	1.038	0.804	0.432	0.496	0.220	0.323	0.342	0.090	0.342	0.350	0.098	0.223	0.215	0.066
		LRB1	1.204	1.752	1.719	0.251	0.251	0.097	0.122	0.128	0.052	0.110	0.113	0.044	0.108	0.110	0.042	0.063	0.066	0.028
		LRB2	1.851	2.311	1.846	0.275	0.276	0.091	0.132	0.140	0.051	0.117	0.125	0.044	0.121	0.123	0.041	0.072	0.075	0.027
	$\Delta_{inter,res}$ (mm)	As-Built	0.143	0.352	0.525	0.108	0.273	0.395	0.027	0.054	0.077	0.012	0.027	0.044	0.012	0.031	0.050	0.007	0.020	0.036
		LRB1	0.162	0.275	0.337	0.016	0.022	0.018	0.012	0.017	0.011	0.003	0.009	0.010	0.009	0.014	0.011	0.004	0.007	0.006
		LRB2	0.164	0.280	0.387	0.011	0.017	0.016	0.010	0.014	0.011	0.003	0.007	0.009	0.009	0.013	0.010	0.003	0.006	0.006
0.8	$\Delta_{inter,max}$ (mm)	As-Built	1.235	1.879	1.773	1.264	1.606	1.375	0.519	0.616	0.284	0.361	0.402	0.111	0.375	0.413	0.118	0.241	0.259	0.081
		LRB1	2.689	3.308	3.165	0.321	0.349	0.222	0.163	0.172	0.073	0.146	0.144	0.052	0.142	0.141	0.049	0.086	0.086	0.032
		LRB2	3.876	4.213	3.285	0.346	0.401	0.273	0.177	0.187	0.084	0.157	0.156	0.058	0.153	0.151	0.055	0.092	0.093	0.037
	$\Delta_{inter,res}$ (mm)	As-Built	0.370	0.812	0.939	0.214	0.635	0.928	0.051	0.093	0.113	0.031	0.048	0.062	0.030	0.051	0.067	0.021	0.039	0.052
		LRB1	0.436	0.760	0.856	0.021	0.058	0.130	0.014	0.023	0.019	0.003	0.011	0.012	0.009	0.016	0.013	0.004	0.008	0.008
		LRB2	0.544	0.803	0.880	0.016	0.066	0.157	0.015	0.020	0.017	0.006	0.010	0.011	0.008	0.015	0.014	0.004	0.008	0.008
1.0	$\Delta_{inter,max}$ (mm)	As-Built	2.014	2.784	2.278	1.572	2.280	2.013	0.607	0.717	0.352	0.393	0.456	0.151	0.411	0.466	0.157	0.261	0.300	0.111
		LRB1	5.220	5.583	5.065	0.407	0.593	0.850	0.218	0.222	0.098	0.181	0.174	0.058	0.177	0.169	0.051	0.105	0.105	0.037
		LRB2	6.537	6.499	4.920	0.440	0.739	1.009	0.235	0.249	0.118	0.198	0.192	0.068	0.190	0.188	0.063	0.116	0.118	0.046
	$\Delta_{inter,res}$ (mm)	As-Built	0.790	1.427	1.515	0.429	1.179	1.579	0.104	0.166	0.184	0.044	0.080	0.091	0.031	0.076	0.093	0.033	0.067	0.076
		LRB1	0.815	1.730	2.713	0.020	0.234	0.782	0.017	0.032	0.041	0.008	0.016	0.018	0.012	0.020	0.019	0.008	0.012	0.016
		LRB2	1.112	1.475	1.660	0.028	0.322	0.938	0.015	0.037	0.047	0.008	0.018	0.024	0.010	0.022	0.025	0.006	0.014	0.024

The statistical investigations of the maximum inter-story drift ratios ($\Delta_{\text{inter,max}}$) for individual frame models under 0.2, 0.6, and 1.0 scale factors are additionally conducted as shown in Figure 18. The as-built frame model is stable up to 0.2 scale factor, and thus has the almost same statistical percentile points distributed over the floors. In contrast, the LRB-isolated models possess the peak maximum inter-story drift ratios that occur at the first floor. The peak maximum inter-story drift ratios at the as-built frame model gradually move into the first floor after reaching 0.6 scale factor applied to the NF ground motions. The increased plastic deformations at the lower stories cause this shift. Although the LRB-isolated frame models possess larger statistical peak ratio points than the as-built frame model, the values of their other statistical ratio points (distributed over from second to top floor) rapidly decrease. A couple of data points shown at the second floor of the as-built frame model exceed 2% drift ratio limit even under 0.6 scale factored ground motions. More severe damages representing larger inter-story drift ratios are found at the first floor of the frame model under 1.0 scale factor. The LRB-isolated frame models have relatively larger maximum inter-story drift ratios distributed over the first floor due to movable base conditions. However, smaller base shear forces transferred from base isolation can cause a huge decrease in the maximum inter-story drift ratios occurring at over second floor. For instance, the median (50th percentile) peak maximum inter-story drift ratios for the LRB1 and LRB2 frame model are 0.41% and 0.44%, respectively, while that for the as-built frame model is 1.57% (see also Table 7).

For another statistical investigation, the residual inter-story drift ratios ($\Delta_{\text{inter,res}}$) for individual frame models under 0.2, 0.6, and 1.0 scale factors are shown in Figure 19. The statistical values for maximum and residual inter-story drift ratios are also summarized in Table 7. For the LRB-isolated frame models, the maximum residual inter-story drift ratios that indicate the most severe damage occurring at the column member are commonly distributed over the first floor. The 84.1 percentile line of the LRB1 frame model starts to exceed the limits for rehabilitation decision (0.5%) under the NF ground motions with 0.6 scale factor, and is slightly larger than that of the LRB2 frame model owing to the implementation of more flexible base isolation systems. In proportion to the rise in the scale factor, the extent of structural damage occurring at the first floor can be also extended with the residual inter-story drift ratio increasing. In spite, these LRB-isolated frame models exhibits excellent recentering properties characterized by the rapidly decreasing residual inter-story drifts that are distributed over upper floors, as compared to the as-built frame model. A couple of data points shown at the third floor of the as-built frame model exceed the rehabilitation decision limit after 1.0 scale factored ground motions (see Figure 19c). Furthermore, the as-built frame model undergoes complete collapse even at the second floor. It can be finally shown that base isolation systems can generally mitigate structural damage generated by the residual inter-story drift.

8. Concluding Remarks

In this study, the LRB isolator devices with the combination of recentering and damping properties are examined for their seismic performance in terms of base shear forces and inter-story drift ratios through nonlinear dynamic time-history analyses with several NF ground motions. The more remarks and conclusions are as follows:

- (1) The force-deformation responses of the LRB models can be idealized as bilinear hysteresis loops simulated based on four main parameters. Two LRB models used in the practical field construction are selected for design and analyses in this study. The LRB2 model was designed with geometric

parameters having larger diameters and smaller heights in comparison to the LRB1 model. For this reason, the LRB2 model exhibits stiffer slope, larger post-yield strength, and slightly lower damping coefficient than the LRB1 model in the force-deformation response curve.

- (2) The prototype buildings constructed as 6 story-braced frame structures can be modeled as 2D numerical frame models because they are designed to be symmetrical to their center axes with uniform mass and stiffness distribution. The LRB isolator devices installed at the column bases of the LRB-isolated frame models were modeled as the nonlinear component springs with behavioral properties. The as-built frame models without base isolation systems had fixed end boundary conditions because their column bases were designed to be fixed.
- (3) A set of 20 NF ground motions were used to conduct the nonlinear dynamic time-history analyses. The average response spectral acceleration for these 20 NF ground motions was investigated to easily estimate base shear forces required for seismic frame design. The band of existing larger spectral accelerations was mostly displayed at the short fundamental time period. Accordingly, the as-built frame model with the short fundamental time period possesses relatively larger response spectral accelerations. The LRB isolator devices can elongate the fundamental time period at the entire frame structure, and effectually mitigate seismic base shear forces transmitted from ground accelerations.
- (4) After conducting time-history analyses with representative NF ground motion data, the seismic responses of the LRB-isolated frame models were compared to those of the as-built frame model in terms of roof displacements, base shear forces, and inter-story drifts. The relatively larger maximum roof displacements were distributed over two LRB-isolated frame models owing to flexible end boundary conditions used for simulating the behavior of the LRB isolator. In spite, these LRB-isolated frame models exhibited smaller residual inter-story drift ratios than the as-built frame model because they were subjected to the mitigated base shear forces transferred from ground accelerations.
- (5) All statistical lines presented herein ascend in the almost straight lines as the scale factor of the ground motion increases. The as-built frame model shows larger maximum and residual inter-story drift ratios as compared to the LRB-isolated frame models under the same seismic loading condition. This implies that the LRB isolator devices reduce the amount of generating base shear forces, thereby mitigating structural damage and permanent deformation occurring over the second floor. Finally, it is concluded based on the analysis result that seismic performance and capacity for the multi-story building structure subjected to severe NF ground motions can be upgraded by installing the LRB isolator devices.

Acknowledgments

This research was supported by Basic Science Research Program through the National Research Foundation of Korea (NRF) funded by the Ministry of Science, ICT, and Future Planning (Grant No. 2013R1A2A2A01068174).

Conflicts of Interest

The author declares no conflict of interest.

References

1. Jangid, R.S.; Kelly, J.M. Base isolation for near-fault motions. *Earthq. Eng. Struct. Dyn.* **2001**, *30*, 691–707.
2. Rodriguez-Marek, A. Near-Fault Seismic Site Response. Ph.D. Thesis, Civil Engineering, University of California, Berkeley, CA, USA, 2000.
3. Providakis, C.P. Effect of LRB isolators and supplemental viscous dampers on seismic isolated buildings under near-fault excitations. *Eng. Struct.* **2008**, *30*, 1187–1198.
4. Baker, J.W. Quantitative classification of near-fault ground motions using wavelet analysis. *Bull. Seismol. Soc. Am.* **2007**, *97*, 1486–1501.
5. Mazza, F.; Vulcano, A. Nonlinear response of RC framed buildings with isolation and supplemental damping at the base subjected to near-fault earthquakes. *J. Earthq. Eng.* **2009**, *13*, 690–715.
6. Mazza, F.; Vulcano, A.; Mazza, F. Nonlinear dynamic response of RC buildings with different base isolation systems subjected to horizontal and vertical components of near-fault ground motions. *Open Constr. Build. Technol. J.* **2012**, *6*, 373–383.
7. Hu, J.W.; Leon, R.T. Analysis and evaluations for composite-moment frames with SMA PR-CFT connections. *Nonlinear Dyn.* **2011**, doi:10.1007/s11071-010-9903-3.
8. Hu, J.W.; Choi, E.; Leon, R.T. Design, analysis, and application of innovative composite PR connections between steel beams and CFT columns. *Smart Mater. Struct.* **2011**, doi:10.1088/0964-1726/20/2/025019.
9. Jangid, R.S. Optimum lead-rubber isolation bearings for near-fault motions. *Eng. Struct.* **2007**, *29*, 2503–2513.
10. Hu, J.W.; Kang, Y.S.; Choi, D.H.; Park, T. Seismic design, performance, and behavior of composite—Moment frames with steel beam-to-concrete filled tube column connections. *KSSC Int. J. Steel Struct.* **2010**, *10*, 177–191.
11. Kelly, J.M. Aseismic base isolation: Review and bibliography. *Soil Dyn. Earthq. Eng.* **1986**, *5*, 202–216.
12. Heaton, T.H.; Hall, J.F.; Wald, D.J.; Halling, M.W. Response of high-rise and base-isolated buildings to a hypothetical Mw 7.0 blind thrust earthquake. *Science* **1995**, *267*, 206–211.
13. Hall, J.F.; Heaton, T.H.; Halling, M.W.; Wald, D.J. Near-source ground motion and its effects on flexible buildings. *Earthq. Spectra* **1995**, *11*, 569–605.
14. Rao, P.B.; Jangid, R.S. Performance of sliding systems under near-fault motions. *Nucl. Eng. Des.* **2001**, *203*, 259–272.
15. Shen, J.; Tsai, M.; Chang, K.; Lee, G.C. Performance of a seismically isolated bridge under near-fault earthquake ground motions. *ASCE J. Struct. Eng.* **2004**, *130*, 861–868.
16. Ahmadi, S.L.; Tadjbakhsh, I.G. A comparative study of performances of various base isolation systems, Part 1: Shear beam structures. *Earthq. Eng. Struct. Dyn.* **1989**, *18*, 11–32.
17. Chen, C.; Yeh, K.; Liu, F. Adaptive fuzzy sliding model control for seismically excited bridges with lead rubber bearing isolation. *Int. J. Uncertain. Fuzz.* **2009**, *17*, 705–727.
18. Lee-Glauser, G.J.; Ahmadi, G.; Horta, L.G. Integrated passive/active vibration absorber for multistory buildings. *ASCE J. Struct. Eng.* **1997**, *123*, 499–504.

19. Su, L.; Ahmadi, G.; Tadjbakhsh, I.G. Comparative study of base isolation systems. *ASCE J. Eng. Mech.* **1989**, *115*, 1976–1992.
20. Robinson, W.H. Lead-rubber hysteretic bearings suitable for protecting structures during earthquakes. *Earthq. Eng. Struct. Dyn.* **1982**, *10*, 593–604.
21. Soong, T.T.; Spencer, B.F. Supplemental energy dissipation: State-of-the-art and state-of-the-practice. *Eng. Struct.* **2002**, *24*, 243–259.
22. American Society of Civil Engineers (ASCE). *Minimum Design Loads for Buildings and Other Structures*; ASCE: Reston, VA, USA, 2005.
23. American Institute of Steel Construction (AISC). *Manual of Steel Construction, Load and Resistance Factor Design (LRFD)*; AISC: Chicago, IL, USA, 2001.
24. International Code Council (ICC). *International Building Code 2006 (IBC2006)*; ICC: Falls Church, VA, USA, 2006.
25. Mazzoni, S.; McKenna, F.; Fenves, G.L. *Open SEES Command Language Manual v. 1.7.3*; Department of Civil Environmental Engineering, University of California: Berkeley, CA, USA, 2006.
26. Newmark, N.M. A method of computation for structural dynamics. *ASCE J. Eng. Mech. Div.* **1959**, *85*, 67–94.
27. Sabelli, R. Research on Improving the Design and Analysis of Earthquake-Resistant Steel-Braced Frames. In *The 2000 NEHRP Professional Fellowship Report*; Earthquake Engineering Research Institute (EERI): Oakland, CA, USA, 2001.
28. Sabelli, R.; Mahin, S.A.; Chang, C. Seismic demands on steel braced-frame buildings with buckling-restrained braces. *Eng. Struct.* **2003**, *25*, 655–666.
29. Somerville, P.G.; Smith, N.; Punyamurthula, S.; Sun, J. *Development of Ground Motion Time Histories for Phase 2 of the FEMA/SAC Steel Project*; SAC Joint Venture: Sacramento, CA, USA, 1997.
30. Mazza, F.; Vulcano, A. Nonlinear dynamic response of r.c. framed structures subjected to near-fault ground motions. *Bull. Earthq. Eng.* **2010**, *8*, 1331–1350.
31. Mollaioli, F.; Lucchini, A.; Cheng, Y.; Monti, G. Intensity measures for the seismic response prediction of base-isolated buildings. *Bull. Earthq. Eng.* **2013**, *11*, 1841–1866.
32. McCormick, J.; Aburano, H.; Ikenaga, M.; Nakashima, M. Permissible residual deformation levels for building structures considering both safety and human elements. In *Proceedings of the 14 World Conference Earthquake Engineering*, Beijing, China, 12–17 October 2008.